

BOOTPLACE: Bootstrapped Object Placement with Detection Transformers

Hang Zhou¹ Xinxin Zuo² Rui Ma^{3†} Li Cheng¹
¹University of Alberta ²Concordia University ³Jilin University

Abstract

In this paper, we tackle the copy-paste image-to-image composition problem with a focus on object placement learning. Prior methods have leveraged generative models to reduce the reliance for dense supervision. However, this often limits their capacity to model complex data distributions. Alternatively, transformer networks with a sparse contrastive loss have been explored, but their over-relaxed regularization often leads to imprecise object placement. We introduce BOOTPLACE, a novel paradigm that formulates object placement as a placement-by-detection problem. Our approach begins by identifying suitable regions of interest for object placement. This is achieved by training a specialized detection transformer on object-subtracted backgrounds, enhanced with multi-object supervisions. It then semantically associates each target composing object with detected regions based on their complementary characteristics. Through a bootstrapped training approach applied to randomly object-subtracted images, our model enforces meaningful placements through extensive paired data augmentation. Experimental results on established benchmarks demonstrate BOOTPLACE’s superior performance in object repositioning, markedly surpassing state-of-the-art baselines on Cityscapes and OPA datasets with notable improvements in IOU scores. Additional ablation studies further showcase the compositionality and generalizability of our approach, supported by user study evaluations. Code is available at <https://github.com/RyanHangZhou/BOOTPLACE>

1. Introduction

Compositional modeling is an emerging research area in both computer vision and computer graphics, focusing on constructing visual scenes by *assembling* components, objects, or elements with precise *placement* and interaction. Task-agnostic approaches, such as image-to-image [22, 51], 3D-object-to-image [18, 47], and 3D-object-to-3D-object [33, 48] composition, have gained wide-ranging

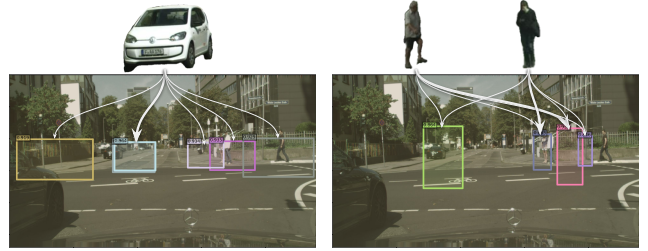


Figure 1. Our approach, BOOTPLACE, *detects* regions of interest (represented as bounding boxes) for object composition and *assigns* each target object to its best-matched detected region. Each object is connected to each detected region with weighted connections, with the bold arrow indicating the strongest link.

applications in content creation [55] and data augmentation [1, 12, 38].

The evolution of image-to-image composition as a standardized input-output interface has enabled precise image editing and enhanced downstream tasks such as semantic segmentation and object detection [13, 53]. Another promising direction involves image-guided composition using diffusion models [8, 17, 29, 40], which excels in blending performance but often struggles to preserve the appearance and orientation of the composed objects.

A key challenge in precise placement learning lies in the difficulty of training models to accurately place objects due to *sparse supervision* of ground-truth location labels. Early approaches addressed this by employing generative models [2, 22, 51, 53] conditioned on joint embeddings of scene images and object patches. These models generated placements using 2D spatial transformations of the object or its bounding box coordinates, bypassing the need for explicit and dense supervision through compositionality-aware saliency maps. Alternatively, transformer-based approaches [55] have been used to regress bounding box placements by directly learning an object-to-background association. This introduces relaxed constraints to mitigate the scarcity of labels. A more recent study [54] increases label availability by manually annotating positive and negative composite pairs, enabling the network to learn to avoid suboptimal object placements. However, the reliance on human-annotation is labor-intensive and prone to inaccuracies, limiting scalability for large-scale applications.

[†]Corresponding author.

In this paper, we present BOOTPLACE, a versatile framework designed to *detect* optimal object placement guided by object queries, and *associate* target compositing object with their best-matched detected region. The detection module is trained on object-subtracted images to identify regions of interest. Region codes learned from this module are independently decoded into bounding-box coordinates and class labels via a feedforward network, resulting in multiple placement predictions. Moreover, to associate the compositing object with its best-matched detected region, we develop a dedicated association network guided by localized semantic complementarity. To address the challenge of label sparsity, we propose a bootstrapped training strategy using randomly object-subtracted images, which enhances data diversification and enables precise object placement.

Our contributions are summarized as follows:

Placement-by-detection framework: We introduce a novel approach for precise object placement by employing detection constraints to identify regions of interest.

Object-to-region association loss: We establish visual correspondences between object queries and local regions of interests in object-subtracted images through an object-to-region associating loss mechanism.

Multi-object placement pipeline: We implement a multi-object placement pipeline, supervised by multi-labels of intact objects, as well as a bootstrapped training strategy to enhance data diversification and improve placement accuracy.

2. Related works

Image composition. Apart from classic methods, including alpha matting [39] and Poisson image editing [34], which seamlessly blend two images, recent works [10, 44] have focused on *harmonizing* the composited region by adjusting its color to better match the background. More recently, there has been a trend towards guided inpainting with visual prompts [8, 30, 40] as a means to achieve more realistic composites. Despite the capabilities of various models to merge two images naturally, these methods all require a bounding box to indicate the target location for the paste. Canet et al. [5] proposed unconstrained compositing by jointly learning object placement and composition. In contrast, our model aims to generate an optimal placement applicable to a variety of composition models.

Object placement. The recent literature has seen significant advancement in the field of learning object placement for copy-paste object compositing, as evidenced by multiple notable works [2, 7, 21, 22, 25, 32, 49, 49, 51, 53–55]. ST-GAN [22] employed an iterative spatial transfor-

mation network to generate a 2D transformation for object placement via adversarial training against a natural image manifold. GCC-GAN [7] incorporated geometric and color consistency in its approach for object placement. Li et al. [21] represented human poses and placement as affordance modeled by variational autoencoders (VAEs). SF-GAN [49] fused geometric and appearance realism within its generator network. Compositional-GAN [2] developed a self-consistent composition-by-decomposition network with a viewpoint-aware appearance flow network to enhance placement. PlaceNet [51] introduced spatial diversity loss for multi-object placement to achieve greater image realism. GracoNet [54] treated object placement as a graph completion problem and employed adversarial training with annotated positive and negative composite pairs. SAC-GAN [53] proposed conditional VAE-GAN for structural coherence via adversarial training against the semantic manifold. TopNet [55] designed a transformer [45] network for object-background correlation with a sparse contrastive loss on placement. DiffPop [25] proposed a plausibility-guided denoising diffusion model to learn the scale and spatial relations among multiple objects and the corresponding scene image. Copy-paste composition also advocates data augmentation for enhancing downstream tasks such as object detection and semantic segmentation [13, 43, 51, 53]. In contrast, our approach learns to detect potential locations for object placement and then associates the compositing object with the best-matched region, demonstrating superior ability to model complex scenes.

Object detection. Modern object detection can be broadly classified into two: two-stage [4, 14, 15, 24, 36] vs single-stage detectors [27, 35, 42]. Typically, these detectors involve heuristic steps such as proposal detection, thresholding, and non-maximum suppression. A significant progress was introduced by DETRs [3, 6, 19, 20, 46, 50], which explored end-to-end object detection using transformers. They treated detection as a set-to-set prediction problem and removed the need for heuristics. In our method, we propose a placement-by-detection paradigm and leverage the detection transformer to enhance the detection ability of the regions of interest.

3. Approach

Our *placement-by-detection* method achieves precise object placement for compositing objects of arbitrary classes. As shown in Figure 2, our approach is structured in two modules: (1) Learning a regions-of-interest detection network for identifying and localizing keyzones suitable for object placement (see Section 3.1), and (2) Leveraging the detected keyzones, learning an object-to-region associating network (see Section 3.2).

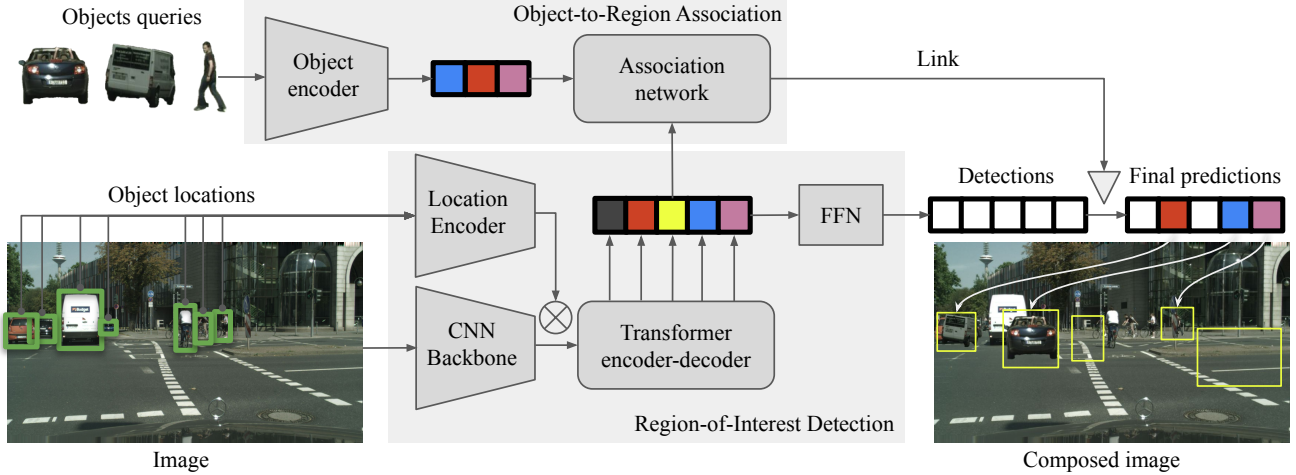


Figure 2. **Network inference.** Given a target image, several object queries (e.g., two cars and a pedestrian) and scene object locations, BOOTPLACE detects a set of candidate region of interest and associates each object with the best-fitting region, which are used to produce the composite image. \otimes is feature concatenation and ∇ is region-wise product.

3.1. Regions-of-interest detection

Let I be an image. The goal of regions-of-interest detection is to identify and localize attentive keyzones. Object detection is its special case where each region of interest is occupied by an individual object. A detector [6, 36, 42] takes the image I as input and produces N region of interest $\{p_i\}$ with locations $\{b_i\}$, $b_i \in \mathbb{R}^4$ and a classification score $s_i \in \mathbb{R}^C$ from a set of predefined classes C as its output. In the first stage, BOOTPLACE detects a fixed set of regions of interest from an object-subtracted image I . Acting as the *occluded context* behind objects, these regions are the *in-painted* version by *removing* objects from the source image. To initiate the object-centric image decomposition process, we perform a series of automated post-processing steps to decompose the source image into an object-subtracted image and a collection of intact object patches: 1) Identify objects with instance segmentation models. 2) Remove objects using dilated masks with image inpainting models. 3) Smooth the image with Gaussian filter to eliminate inpainting artifacts. This image decomposition process is visualized in Figure 3 and detailed in [supplementary](#).

Our detection model is built upon detection transformers, consisting of a CNN backbone for generating a lower-resolution image embedding, a multi-layer Transformer encoder to produce a compact image embedding, a multi-layer Transformer decoder that applies multi-headed self- and encoder-decoder attention using a set of learnable queries to generate output embeddings, and multiple prediction heads. To prevent compositing objects from being placed over existing scene objects, the locations of these scene objects are encoded into the network to guide placement. Specifically, scene object locations are encoded by an MLP-based location encoder, then concatenated with image features to form location-aware image features.

3.2. Object-to-region associating network

In addition to the detection objective, we aim to equip our detector with the ability to understand the relations between regions of interest and compositing objects. In the second stage, BOOTPLACE learns an object-to-region associating network using the detected keyzones and corresponding object patches from the first stage.

Our associating network associates regions of interest with object patches in a probabilistic and differentiable manner. Formally, each object query q_k links region of interest p_i , and produces an object association score vector $g \in \mathbb{R}^N$ over a collection of region of interest. This association score vector then yields an association $\alpha_k \in \{\emptyset, 1, 2, \dots, N\}$ where N is the number of detected regions of interest in the image I . The association then links ground-truth location τ_k to current detected regions of interest p_i , and is given by:

$$\tau_k = \begin{cases} \emptyset, & \text{if } \alpha = \emptyset \\ b_{\alpha_k}, & \text{otherwise} \end{cases} \quad (1)$$

where $\alpha = \emptyset$ indicates no association. Notably, the association step is differentiable and can be jointly trained with the underlying detector network.

The association score is elaborated as follows. Let p_1, \dots, p_N be a set of high-confidence regions of interest for image I . Let $B = \{b_1, \dots, b_N\}$ be their corresponding bounding boxes. Let $f_i \in \mathbb{R}^D$ be the D -dimensional features extracted from each region of interest. For convenience let $F = \{f_1, \dots, f_N\}$ be the set of all detection features of image I . The associating network takes object features F and an image I , and produces an object-specific association score $g(q_k, F) \in \mathbb{R}^N$. Let $g_i(q_k, F) \in \mathbb{R}$ be the score of the i -th region of interest in the image. A special

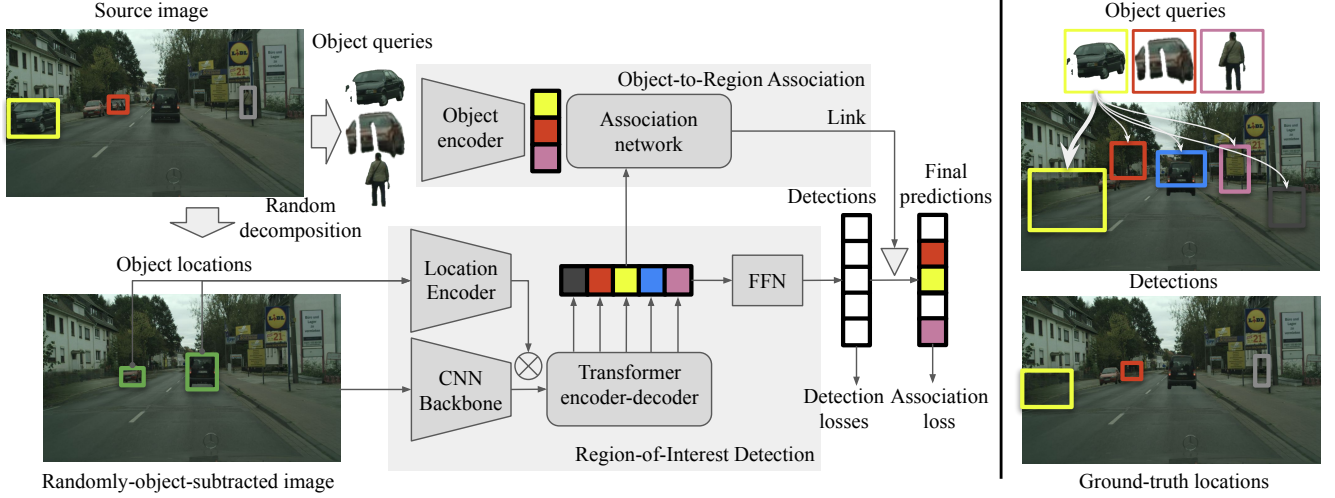


Figure 3. **Network architecture and training.** We prepare training data by first decomposing a source image into a randomly-object-subtracted image \mathcal{I} and a set of object queries. During training, image I and scene object locations are both fed into a detection transformer for region-of-interest detection. The object queries are fed into an association network for object-to-region matching, where the generated association links each object query with the detected region of interest. Losses comprises of detection loss and association loss. At the high level, we visualize the relations among object queries, detected regions of interest and ground-truth locations on the right side, where the best-matched association arrow is highlighted in bold.

output token $g_0(q_k, F) = 0$ indicates no association. The associating network then outputs a distribution of associations over all regions of interest in the image for each object patch q_k . We model this by softmax activation:

$$P_A(\alpha = i|F) = \frac{\exp(g_i(q_k, F))}{\sum_{j \in \{0, 1, 2, \dots, N\}} \exp(g_j(q_k, F))}. \quad (2)$$

Instead of just a dot-product association score between the object query and region-of-interest feature $g_i(q_k, F)$, to avoid the association with scene objects, we propose incorporating negative correlations rather than positive correlations for *semantic complementary*, providing the model with a nuanced understanding and enhancing its ability to recognize optimal placement regions within the scene.

$$g_i(q_k, F) = -q_k \cdot F_i / \mu, \quad (3)$$

where μ is a temperature parameter. During training, we maximize the log-likelihood of the ground-truth object-to-region association. During inference, we use the likelihood to find the best-matched object-to-region association.

Network structure. The object-to-region association comprises a CNN-based object encoder network for extracting object embeddings, and an association module that takes a stack of region-of-interest features $F \in \mathbb{R}^{N \times D}$ and a matrix of object query features $Q \in \mathbb{R}^{T \times D}$ as two inputs and produces an association matrix $G \in \mathbb{R}^{T \times N}$ between queries and regions of interest with cosine similarity.

3.3. Training

Given ground-truth bounding box locations $\tau_1, \tau_2, \dots, \tau_T$ where $\tau_k \in \mathbb{R}^4 \cup \emptyset$ and corresponding classes c_1, c_2, \dots, c_T , the goal is to learn an associating network that estimates P_A . The associating network and the detection transformer are jointly trained, with the association network functioning as a region-of-interest head, similar to two-stage detectors [36]. During each training iteration, high-confidence regions of interest b_1, \dots, b_N along with their corresponding features F and class prediction s_1, s_2, \dots, s_N are first obtained. For each sample, $P_A(\alpha|F)$ is then maximized.

Following DETR [6], both the class prediction and the similarity of predicted and ground-truth boxes are taken into account for the assignment rule. Specifically, each element k of the ground-truth set can be seen as a (c_k, τ_k) where c_k is the target class label (which may be \emptyset). For the prediction with index (association) α_k , the probability of class c_k is defined as $P_{\alpha_k}(c_k)$ and the predicted box as b_{α_k} .

With these notations, the association cost between the ground truth and the prediction with index α_k is defined as

$$L_{cost}(\tau_k, c_k, P_{\alpha_k}(c_k), b_{\alpha_k}) = -\mathbb{1}_{c_k \neq \emptyset} P_{\alpha_k}(c_k) + \mathbb{1}_{c_k \neq \emptyset} L_{box}(\tau_k, b_{\alpha_k}). \quad (4)$$

To find a one-to-one bipartite matching between predicted boxes and ground-truth boxes, a permutation of T elements with the lowest cost is searched:

$$\hat{\alpha} = \arg \max_{\alpha} \sum_k^T L_{cost}(\tau_k, c_k, P_{\alpha_k}(c_k), b_{\alpha_k}). \quad (5)$$

This optimal assignment $\hat{\alpha}$ could be computed efficiently with the Hungarian algorithm, and is used to both train the bounding box regression of the underlying two-stage detector, and our assignment likelihood P_A .

Bootstrapped training strategy. To enhance the diversity of training data, a bootstrapped strategy is employed for augmenting training data, as shown in Figure 3. Specifically, having T intact objects subtracted from an image, a subset of objects is randomly selected and is recomposed back to the object-subtracted image to create a randomly-object-subtracted image \mathcal{I} . The remaining objects are viewed as target compositing objects. Through this process, we expand the training data from a single scenario to a comprehensive set of combinations, reaching a total of $\sum_{i=1}^T \binom{T}{i}$ samples for each scene. This strategy significantly enriches the training dataset, exposing the model to a more extensive variety of scenarios.

The overall training losses includes the assignment from Equation (5) and an association loss for all compositing objects. The association loss is defined as the sum of the log-likelihood of the assignments α_k of each location τ_k :

$$L_{asso}(F, \{\tau_1, \tau_2, \dots, \tau_T\}) = - \sum_{k=1}^T \log P_A(\hat{\alpha}_k | F). \quad (6)$$

We train \mathcal{L}_{asso} jointly with standard detection losses [6], including classification loss \mathcal{L}_{cls} and bounding-box regression loss \mathcal{L}_{box} [37]:

$$\mathcal{L} = \mathcal{L}_{cls} + \alpha \mathcal{L}_{box} + \beta \mathcal{L}_{asso}. \quad (7)$$

4. Experiments

Datasets. We conducted experiments on Cityscapes [11] and OPA [26] datasets. Cityscapes is a large-scale urban street dataset for semantic segmentation. We use MaskFormer [9] to obtain individual objects with panoptic segmentation, and background images by removing objects and their shadows with pretrained LaMa inpainting model [41] and online PhotoKit¹ tool. After data cleaning, we build a multiple-object placement dataset containing 2,953 training images with 22,270 objects and their ground-truth labels, and 372 testing images with 2,713 objects. OPA is a human-annotated composite dataset collected from COCO [23] dataset for object placement. It contains 62,074 training images and 11,396 test images without overlap. We only use positive samples, which consist of 21,350 pairs of images and objects for training and 3,566 pairs for testing.

Implementation details. We train BOOTPLACE with AdamW [28] optimizer with an initial learning rate of

0.0004, the backbone’s to 0.00005 and weight decay to 0.0001. By default, we set $\alpha = 5$, $\beta = 1$, $\mu = 0.07$, and Gaussian filter with $\sigma = 5$. Training on Cityscapes dataset takes 12 hours on one NVIDIA TITAN RTX GPU, and 8 hours for OPA dataset.

Evaluation. We quantitatively evaluate object reposition accuracy using top- k intersection-over-union (IOU) on all output bounding boxes and evaluate detection precision with IOU50. For object placement, we measure *plausibility* by a user study involving 20 participants who compare the realism of composite images generated by different methods using the same object patches and backgrounds, and *diversity* via standard deviation of bbox scale, x-center, and y-center with the trial number set to 5. Users were asked to focus on structural consistency instead of factors such as image resolution or color consistency. Unlike previous methods that relied on FID [16] or LPIPS [52], we find these metrics less accurate due to their inability to reflect regional boundary artifacts and resolution variations.

4.1. Comparisons with previous methods

Object reposition. Object reposition refers to object placement where the object patch and background are from the same image. In Table 1, we compare the object reposition accuracy with PlaceNet [51], GracoNet [54], SAC-GAN [53] and TopNet [55]. We observe that BOOTPLACE shows significant performance advantages compared to other methods, with a 4% improvement in top-5 IOU over TopNet, the state-of-the-art method. Our BOOTPLACE is more accurate at repositioning objects back onto backgrounds, in that it leverages the detection transformer’s strong capability for precise localization. The visual results in Figures 4 and 5 also illustrate the enhanced object placement performance achieved by our method. We notice that placing objects with distinct orientations, such as a car in a road scene, is more challenging than positioning generic objects as the orientation of the object must align with the semantic cues in the image, such as the direction of the road. It is also worth noting that when training our method on the OPA dataset, we only used single-object labels for supervision due to the lack of multi-object annotations. Despite this limitation, our method still performs better than others.

Object placement. We perform object placement experiments on composing moving objects (e.g., cars, buses and trucks) into images from Cityscapes. In Table 2, we compare qualitative results with PlaceNet, SAC-GAN and TopNet, observing that our BOOTPLACE significantly outperforms others. As shown in Figure 6, our method produces diverse and accurate placements, while previous methods often result in object collisions, incorrect placements, or inconsistent scales. GracoNet was excluded from evaluation

¹<https://photokit.com/>

	Cityscapes				OPA			
	IOU50@1 (\uparrow)	IOU@1 (\uparrow)	IOU50@5 (\uparrow)	IOU@5 (\uparrow)	IOU50@1 (\uparrow)	IOU@1 (\uparrow)	IOU50@5 (\uparrow)	IOU@5 (\uparrow)
PlaceNet (ECCV'20) [51]	0	0.045	0	0.045	2.76	0.116	10.09	0.225
GracoNet (ECCV'22) [54]	—	—	—	—	2.49	0.131	16.60	0.248
SAC-GAN (IEEE TVCG'22) [53]	0.806	0.082	1.08	0.085	—	—	—	—
TopNet (CVPR'23) [55]	0.807	0.045	1.61	0.070	11.55	0.197	15.95	0.241
BOOTPLACE (ours)	1.74	0.197	6.09	0.281	11.60	0.197	22.41	0.281

Table 1. **Quantitative results of object reposition** on Cityscapes and OPA datasets, evaluated by IOU50 (%), top-1 and top-5 IOU.

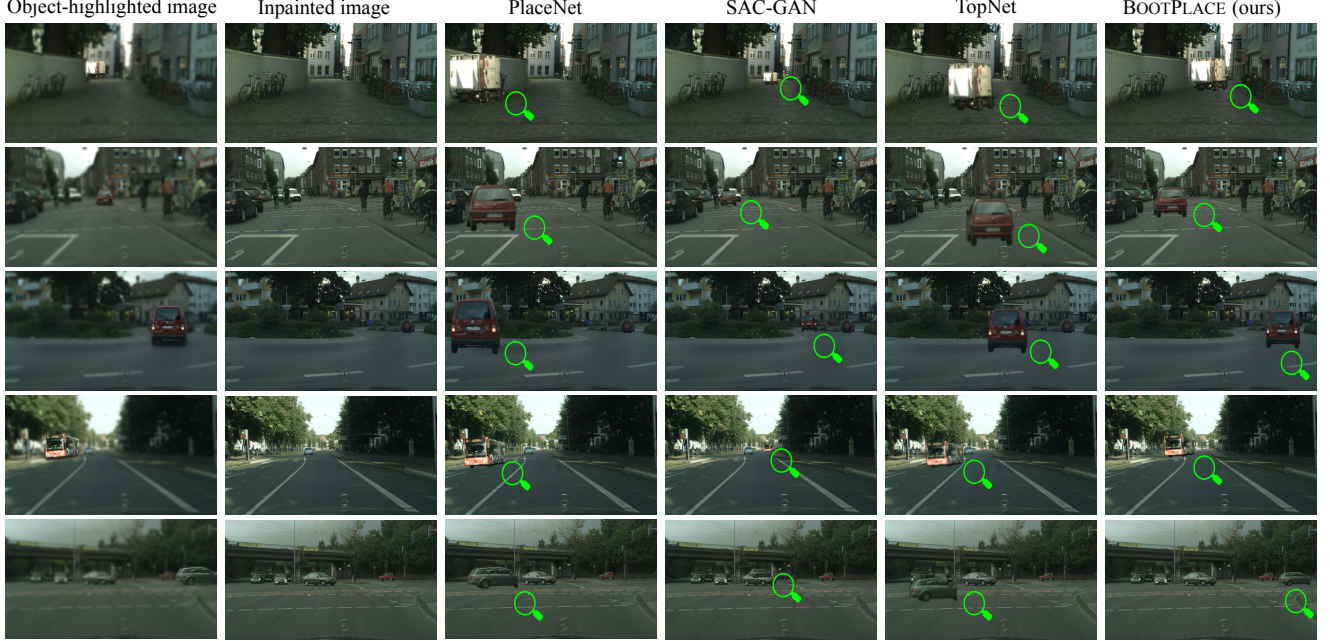


Figure 4. **Qualitative results of object reposition** on Cityscapes dataset. Zoom in to see visual details. 1st column: original images with highlighted compositing objects; 2nd column: inpainted images after object subtraction.

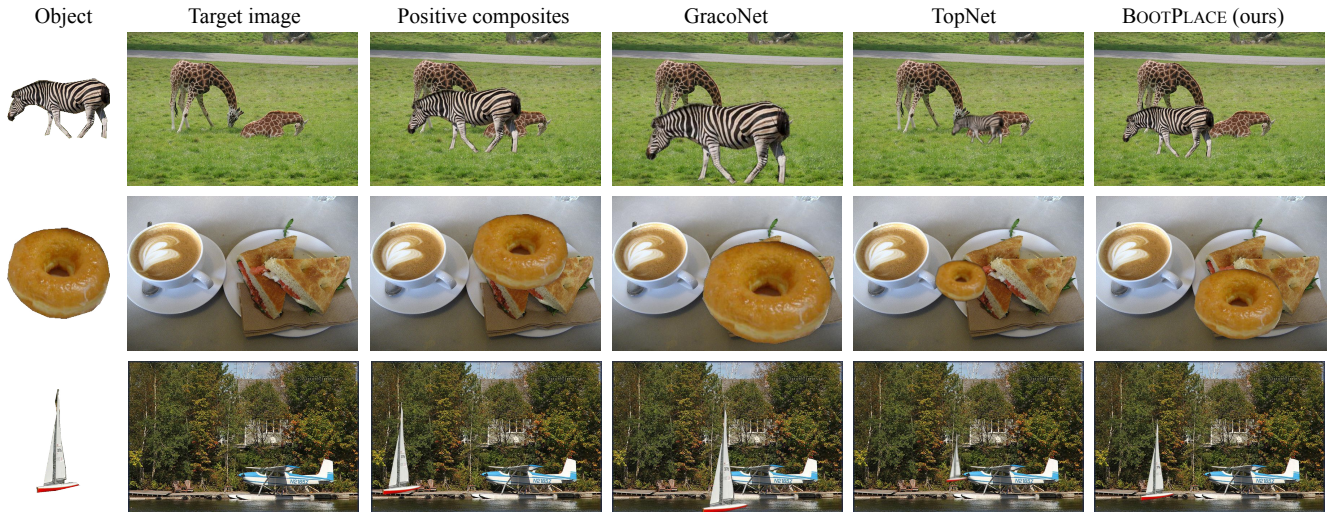


Figure 5. **Qualitative results of object reposition** on OPA dataset. “Positive composites” are annotated good-quality composites from OPA. SAC-GAN is excluded as it requires semantic maps for training.

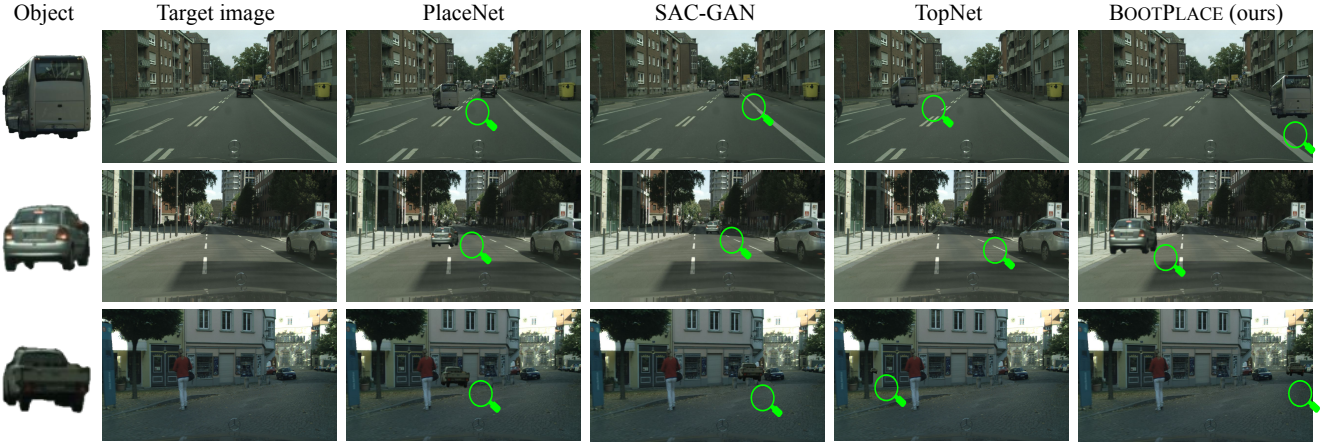


Figure 6. **Qualitative results of object placement** on Cityscapes dataset. Objects are randomly chosen from Cityscapes testing set.

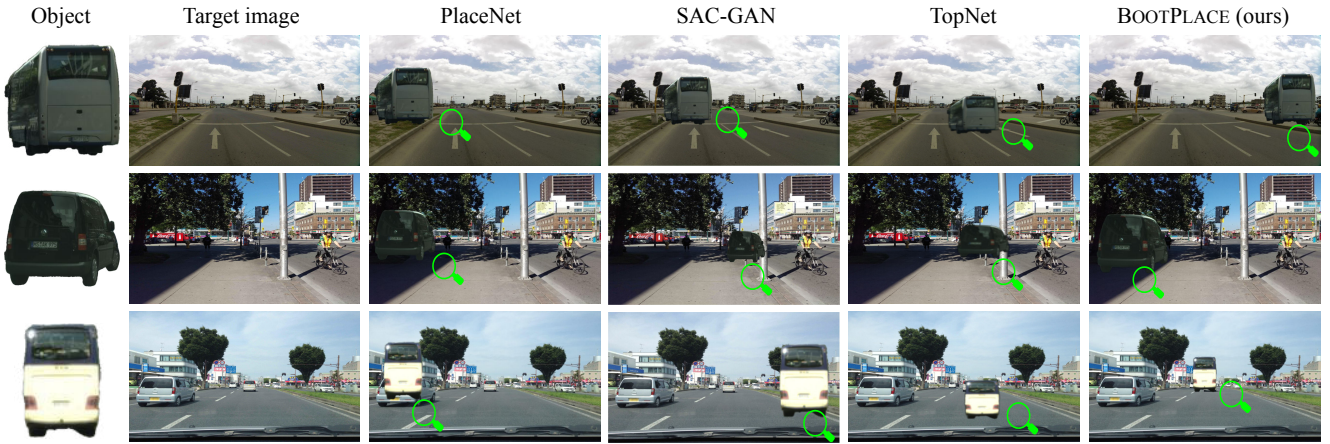


Figure 7. **Qualitative results of object placement** on Mapillary Vistas dataset. Objects are randomly chosen from Cityscapes testing set.

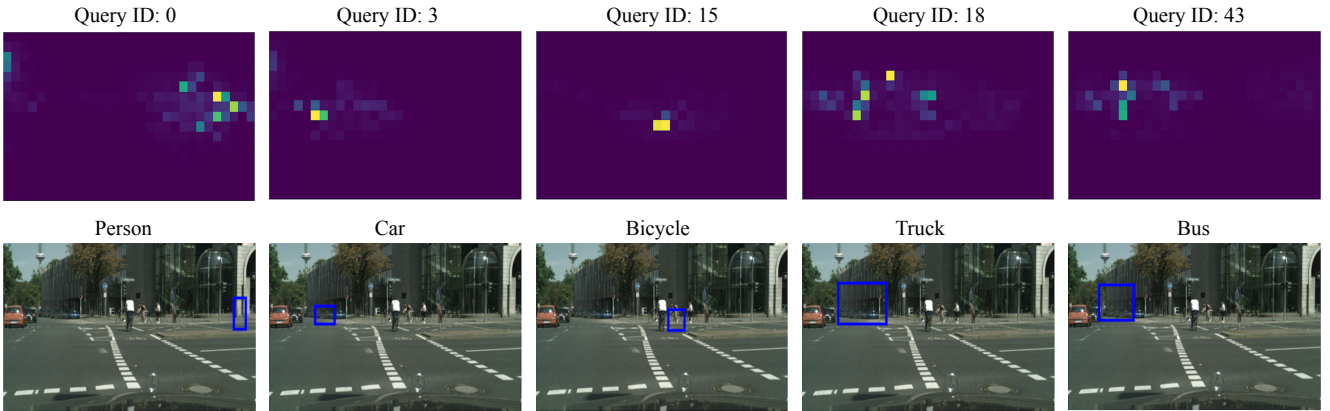


Figure 8. **Visualizing decoder attention** for every detected region for object placement (images from Cityscapes val set), which part of the image the model was looking at to predict this specific bounding box and class. Best viewed in color.

as it requires negative composite images for training, which is unavailable in the Cityscapes dataset. For PlaceNet, we have dropped its diverse loss during training, as it is specif-

ically designed for multi-object placement. In addition, we compare the *scalability* of different models by testing the placement performance on Mapillary Vistas [31] images us-

	Plausibility User study (†)		Diversity Mean±std (†)	x-center	y-center
	Cityscapes	MV			
PlaceNet [51]	0.183	0.133	0.204±0.0008	0.287±0.0018	0.465±0.0005
SAC-GAN [53]	0.269	0.285	0.156±0.0092	0.488±0.0405	0.436±0.0056
TopNet [55]	0.246	0.260	0.079±0.0131	0.372±0.0818	0.464±0.0138
BOOTPLACE (ours)	0.303	0.323	0.310±0.1235	0.255±0.1082	0.495±0.0328

Table 2. **Quantitative comparisons of car placement** on Cityscapes and Mapillary Vistas (MV) datasets.

	W/o smooth.	W/o augment.	Pos. contrast.	Single label	W/o LE	Full model
IOU50@1 (†)	0	0.94	1.88	0	0	1.74
IOU@1 (†)	0	0.056	0.049	0.167	0.069	0.197
IOU50@5 (†)	4.23	3.29	4.69	2.61	0	6.09
IOU@5 (†)	0.082	0.121	0.125	0.239	0.086	0.281

Table 3. **Ablation study** of object reposition on Cityscapes [11] dataset, evaluated by IOU50 (%), top-1 and top-5 IOU. LE stands for location encoder.

ing models trained on the Cityscapes dataset; see Table 2 and Figure 7. Our BOOTPLACE exhibits superior scalability than other methods.

4.2. Overfitting to inpainting artifact?

Although we have applied Gaussian blur and multi-region inpainting to reduce the impact of inpainting artifacts on object placement, our model potentially overfits to the regions. In Figure 9, we show the *overfitting rate* across IOU thresholds for different top- k predictions. At IOU50, the rate remains below 0.05, confirming our method exhibits minimal overfitting to artifacts.

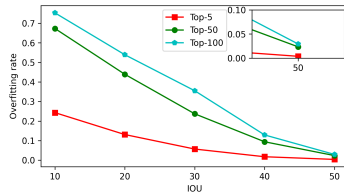


Figure 9. Overfitting rate vs IOU.

4.3. Ablation study

In Table 3, we compare our method with several variations: a) no Gaussian smoothing; b) no bootstrapped data augmentation; c) using positive correlations; d) single-object supervision; (e) no location encoder; (f) full model. The results support our design choices for individual modules. Gaussian smoothing is crucial in preventing overfitting to inpainting artifacts and pixel variations. Data augmentation leads to a 0.17 improvement in IOU@5. Negative correlations help our network avoid placing compositing objects over existing objects in the scene, thereby preventing unwanted occlusions. The full multiple-object supervision outperforms the single-object supervision, with IOU@5 increased by 0.042. The explicit location input significantly improves reposition accuracy by constraining the detection space, with IOU@5 increased by 0.195.

Bounding box distribution. We visualize *bbox distributions* in Figure 10 for object placement in Cityscapes images and observe that our method identifies more diverse

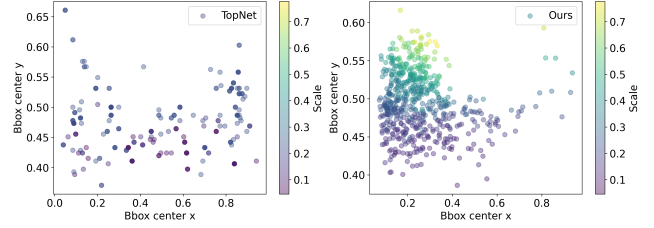


Figure 10. Bbox distribution. Color intensity reflects bbox scales.



Figure 11. **Failure cases.** Composed objects are rendered in blue.

ROIs than TopNet. Our method sufficiently covers a wide range of reasonable locations, therefore cases of reasonable placements being missed are less likely to occur.

Decoder attention visualization. In Figure 8, we visualize the decoder attention of our trained model, revealing that the model attends to different regions for detecting objects of different categories. We observe that the decoder’s attention tends to focus on local extremities. The attention visualization aligns with our expectations: different queries detect different locations, such as vehicles being placed near the roadside or other vehicles, pedestrians being placed along the sidewalk, and bicycles either riding on the road or parked at the street side.

5. Discussions, limitations and future work

We have introduced BOOTPLACE, a placement-by-detection paradigm based on detection transformers and association networks. By leveraging multi-object supervision to detect regions of interest, our approach significantly enhances object placement performance. The proposed association network enables the differentiable association between compositing objects and the detected regions. Additionally, we introduce a bootstrapped training strategy that increases data diversity.

Similar to most object detection methods, our approach detects locations *in parallel*, limiting its suitability for sequential object placement. As shown in Figure 11, this leads to undesirable occlusions, such as a car colliding with a curb (left) and overlapping cars (right). Additionally, most object placement methods lack out-of-plane rotation and perspective transformation modeling, resulting in less realistic compositions. To overcome these challenges, we intend to develop autoregressive models to better handle the sequential object placement problem.

Acknowledgments

This work was partly supported by NSERC Discovery, CFI-JELF, NSERC Alliance, Alberta Innovates and PrairiesCan grants. Part of this work was conducted at the Simon Fraser University and we thank Prof. Hao Zhang for insightful discussions.

References

- [1] Antreas Antoniou, Amos Storkey, and Harrison Edwards. Data augmentation generative adversarial networks. *arXiv preprint arXiv:1711.04340*, 2017. 1
- [2] Samaneh Azadi, Deepak Pathak, Sayna Ebrahimi, and Trevor Darrell. Compositional GAN: Learning image-conditional binary composition. *IJCV*, 2020. 1, 2
- [3] Quentin Bouniot, Romaric Audigier, Angélique Loesch, and Amaury Habrard. Proposal-contrastive pretraining for object detection from fewer data. In *ICLR*, 2023. 2
- [4] Zhaowei Cai and Nuno Vasconcelos. Cascade R-CNN: Delving into high quality object detection. In *CVPR*, 2018. 2
- [5] Gemma Canet Tarrés, Zhe Lin, Zhifei Zhang, Jianming Zhang, Yizhi Song, Dan Ruta, Andrew Gilbert, John Colloso, and Soo Ye Kim. Thinking Outside the BBox: Unconstrained generative object compositing. In *ECCV*, 2024. 2
- [6] Nicolas Carion, Francisco Massa, Gabriel Synnaeve, Nicolas Usunier, Alexander Kirillov, and Sergey Zagoruyko. End-to-end object detection with transformers. In *ECCV*, 2020. 2, 3, 4, 5
- [7] Bor-Chun Chen and Andrew Kae. Toward realistic image compositing with adversarial learning. In *CVPR*, 2019. 2
- [8] Xi Chen, Lianghua Huang, Yu Liu, Yujun Shen, Deli Zhao, and Hengshuang Zhao. AnyDoor: Zero-shot object-level image customization. In *CVPR*, 2024. 1, 2
- [9] Bowen Cheng, Alex Schwing, and Alexander Kirillov. Per-pixel classification is not all you need for semantic segmentation. *NeurIPS*, 2021. 5, 1
- [10] Wenyan Cong, Jianfu Zhang, Li Niu, Liu Liu, Zhixin Ling, Weiyuan Li, and Liqing Zhang. DoveNet: Deep image harmonization via domain verification. In *CVPR*, 2020. 2
- [11] Marius Cordts, Mohamed Omran, Sebastian Ramos, Timo Rehfeld, Markus Enzweiler, Rodrigo Benenson, Uwe Franke, Stefan Roth, and Bernt Schiele. The Cityscapes dataset for semantic urban scene understanding. In *CVPR*, 2016. 5, 8, 1
- [12] Debidatta Dwibedi, Ishan Misra, and Martial Hebert. Cut, paste and learn: Surprisingly easy synthesis for instance detection. In *ICCV*, 2017. 1
- [13] Golnaz Ghiasi, Yin Cui, Aravind Srinivas, Rui Qian, Tsung-Yi Lin, Ekin D Cubuk, Quoc V Le, and Barret Zoph. Simple copy-paste is a strong data augmentation method for instance segmentation. In *CVPR*, 2021. 1, 2
- [14] Ross Girshick. Fast R-CNN. In *ICCV*, 2015. 2
- [15] Ross Girshick, Jeff Donahue, Trevor Darrell, and Jitendra Malik. Rich feature hierarchies for accurate object detection and semantic segmentation. In *CVPR*, 2014. 2
- [16] Martin Heusel, Hubert Ramsauer, Thomas Unterthiner, Bernhard Nessler, and Sepp Hochreiter. GANs trained by a two time-scale update rule converge to a local Nash equilibrium. *NeurIPS*, 2017. 5
- [17] Jonathan Ho, Ajay Jain, and Pieter Abbeel. Denoising diffusion probabilistic models. *NeurIPS*, 2020. 1
- [18] Yannick Hold-Geoffroy, Akshaya Athawale, and Jean-François Lalonde. Deep sky modeling for single image outdoor lighting estimation. In *CVPR*, 2019. 1
- [19] Aishwarya Kamath, Mannat Singh, Yann LeCun, Gabriel Synnaeve, Ishan Misra, and Nicolas Carion. MDETR-modulated detection for end-to-end multi-modal understanding. In *ICCV*, 2021. 2
- [20] Liunian Harold Li, Pengchuan Zhang, Haotian Zhang, Jianwei Yang, Chunyuan Li, Yiwu Zhong, Lijuan Wang, Lu Yuan, Lei Zhang, Jenq-Neng Hwang, et al. Grounded language-image pre-training. In *CVPR*, 2022. 2
- [21] Xueting Li, Sifei Liu, Kihwan Kim, Xiaolong Wang, Ming-Hsuan Yang, and Jan Kautz. Putting humans in a scene: Learning affordance in 3D indoor environments. In *CVPR*, 2019. 2
- [22] Chen-Hsuan Lin, Ersin Yumer, Oliver Wang, Eli Shechtman, and Simon Lucey. ST-GAN: Spatial transformer generative adversarial networks for image compositing. In *CVPR*, 2018. 1, 2
- [23] Tsung-Yi Lin, Michael Maire, Serge Belongie, James Hays, Pietro Perona, Deva Ramanan, Piotr Dollár, and C Lawrence Zitnick. Microsoft COCO: Common objects in context. In *ECCV*, 2014. 5
- [24] Tsung-Yi Lin, Piotr Dollár, Ross Girshick, Kaiming He, Bharath Hariharan, and Serge Belongie. Feature pyramid networks for object detection. In *CVPR*, 2017. 2
- [25] Jiacheng Liu, Hang Zhou, Shida Wei, and Rui Ma. DiffPop: Plausibility-guided object placement diffusion for image composition. *Computer Graphics Forum*, 2024. 2
- [26] Liu Liu, Zhenchen Liu, Bo Zhang, Jiangtong Li, Li Niu, Qingyang Liu, and Liqing Zhang. OPA: Object placement assessment dataset. *arXiv preprint arXiv:2107.01889*, 2021. 5
- [27] Wei Liu, Dragomir Anguelov, Dumitru Erhan, Christian Szegedy, Scott Reed, Cheng-Yang Fu, and Alexander C Berg. SSD: Single shot multibox detector. In *ECCV*, 2016. 2
- [28] Ilya Loshchilov and Frank Hutter. Decoupled weight decay regularization. In *ICLR*, 2018. 5
- [29] Shilin Lu, Yanzhu Liu, and Adams Wai-Kin Kong. TF-ICON: Diffusion-based training-free cross-domain image composition. In *ICCV*, 2023. 1
- [30] Chenlin Meng, Yutong He, Yang Song, Jiaming Song, Jiajun Wu, Jun-Yan Zhu, and Stefano Ermon. SDEdit: Guided image synthesis and editing with stochastic differential equations. In *ICLR*, 2021. 2
- [31] Gerhard Neuhold, Tobias Ollmann, Samuel Rota Buló, and Peter Kontschieder. The Mapillary Vistas Dataset for semantic understanding of street scenes. In *ICCV*, 2017. 7
- [32] Li Niu, Qingyang Liu, Zhenchen Liu, and Jiangtong Li. Fast object placement assessment. *arXiv preprint arXiv:2205.14280*, 2022. 2

- [33] Wamiq Reyaz Para, Paul Guerrero, Niloy Mitra, and Peter Wonka. COFS: Controllable furniture layout synthesis. In *SIGGRAPH*, 2023. 1
- [34] Patrick Pérez, Michel Gangnet, and Andrew Blake. Poisson image editing. In *SIGGRAPH*, 2003. 2
- [35] Joseph Redmon, Santosh Divvala, Ross Girshick, and Ali Farhadi. You Only Look Once: Unified, real-time object detection. In *CVPR*, 2016. 2
- [36] Shaoqing Ren, Kaiming He, Ross Girshick, and Jian Sun. Faster R-CNN: Towards real-time object detection with region proposal networks. *NeurIPS*, 2015. 2, 3, 4
- [37] Hamid Rezaatoughi, Nathan Tsoi, JunYoung Gwak, Amir Sadeghian, Ian Reid, and Silvio Savarese. Generalized intersection over union: A metric and a loss for bounding box regression. In *CVPR*, 2019. 5
- [38] Connor Shorten and Taghi M Khoshgoftaar. A survey on image data augmentation for deep learning. *Journal of Big Data*, 2019. 1
- [39] Alvy Ray Smith and James F Blinn. Blue screen matting. In *SIGGRAPH*, 1996. 2
- [40] Yizhi Song, Zhifei Zhang, Zhe Lin, Scott Cohen, Brian Price, Jianming Zhang, Soo Ye Kim, and Daniel Aliaga. Object-Stitch: Object compositing with diffusion model. In *CVPR*, 2023. 1, 2, 3
- [41] Roman Suvorov, Elizaveta Logacheva, Anton Mashikhin, Anastasia Remizova, Arsenii Ashukha, Aleksei Silvestrov, Naejin Kong, Harshith Goka, Kiwoong Park, and Victor Lempitsky. Resolution-robust large mask inpainting with fourier convolutions. In *WACV*, 2022. 5, 1
- [42] Zhi Tian, Chunhua Shen, Hao Chen, and Tong He. FCOS: Fully convolutional one-stage object detection. In *ICCV*, 2019. 2, 3
- [43] Shashank Tripathi, Siddhartha Chandra, Amit Agrawal, Ambrish Tyagi, James M Rehg, and Visesh Chari. Learning to generate synthetic data via compositing. In *CVPR*, 2019. 2
- [44] Yi-Hsuan Tsai, Xiaohui Shen, Zhe Lin, Kalyan Sunkavalli, Xin Lu, and Ming-Hsuan Yang. Deep image harmonization. In *CVPR*, 2017. 2
- [45] Ashish Vaswani, Noam Shazeer, Niki Parmar, Jakob Uszkoreit, Llion Jones, Aidan N Gomez, Łukasz Kaiser, and Illia Polosukhin. Attention is all you need. *NeurIPS*, 2017. 2
- [46] Pei Wang, Zhaowei Cai, Hao Yang, Gurumurthy Swaminathan, Nuno Vasconcelos, Bernt Schiele, and Stefano Soatto. Omni-DETR: Omni-supervised object detection with transformers. In *CVPR*, 2022. 2
- [47] Zian Wang, Wenzheng Chen, David Acuna, Jan Kautz, and Sanja Fidler. Neural light field estimation for street scenes with differentiable virtual object insertion. In *ECCV*, 2022. 1
- [48] Qihong Anna Wei, Sijie Ding, Jeong Joon Park, Rahul Sajnani, Adrien Poulénard, Srinath Sridhar, and Leonidas Guibas. LEGO-Net: Learning regular rearrangements of objects in rooms. In *CVPR*, 2023. 1
- [49] Fangneng Zhan, Hongyuan Zhu, and Shijian Lu. Spatial fusion GAN for image synthesis. In *CVPR*, 2019. 2
- [50] Hao Zhang, Feng Li, Shilong Liu, Lei Zhang, Hang Su, Jun Zhu, Lionel M Ni, and Heung-Yeung Shum. DINO: DETR with improved denoising anchor boxes for end-to-end object detection. In *ICLR*, 2023. 2
- [51] Lingzhi Zhang, Tarmily Wen, Jie Min, Jiancong Wang, David Han, and Jianbo Shi. Learning object placement by inpainting for compositional data augmentation. In *ECCV*, 2020. 1, 2, 5, 6, 8, 3
- [52] Richard Zhang, Phillip Isola, Alexei A Efros, Eli Shechtman, and Oliver Wang. The unreasonable effectiveness of deep features as a perceptual metric. In *CVPR*, 2018. 5
- [53] Hang Zhou, Rui Ma, Ling-Xiao Zhang, Lin Gao, Ali Mahdavi-Amiri, and Hao Zhang. SAC-GAN: Structure-aware image composition. *IEEE TVCG*, 2022. 1, 2, 5, 6, 8, 3
- [54] Siyuan Zhou, Liu Liu, Li Niu, and Liqing Zhang. Learning object placement via dual-path graph completion. In *ECCV*, 2022. 1, 2, 5, 6
- [55] Sijie Zhu, Zhe Lin, Scott Cohen, Jason Kuen, Zhifei Zhang, and Chen Chen. TopNet: Transformer-based object placement network for image compositing. In *CVPR*, 2023. 1, 2, 5, 6, 8, 3

BOOTPLACE: Bootstrapped Object Placement with Detection Transformers

Supplementary Material

6. Network and parameter details

For the image encoder, We use ImageNet-pretrained ResNet-50 with frozen batchnorm layers and discard the last classification layer as the CNN backbone. The Transformer encoder contains 6 blocks and the Transformer decoder contains 6 block. Each attention layer has 8 attention heads. Additive dropout of 0.1 is applied after every multi-head attention and FFN before layer normalization. The weights are randomly initialized with Xavier initialization. The intermediate size of the feedforward layers in the transformer blocks is set 2048 and the size of the embeddings d in the transformer is set 256. The number of object (region) queries N is set to 100 and the maximum number of objects M is set to 120. For the bounding box encoder, we utilize 2-layer MLP which transforms the bounding box embedding into 256 dimension and multiple it with the embedding obtained from the Transformer decoder, and then use 3-layer MLP to map it to 4-dim embeddings.

7. Computational cost

To compare the computation costs of different methods, we show the number of Params, FLOPs and inference time of PlaceNet, SAC-GAN, TopNet and BOOTPLACE in Table 4. Our method requires slightly more parameters than the other methods. The theoretical computation cost (FLOPs) of our method is 7x larger, but is similar to DETR-based detection models. We also tested the inference time on the Cityscapes validation set using an Nvidia GeForce GTX TITAN X with a batch size of 1. The inference time per sample of our method is less than 1 second, significantly faster than TopNet (2.7 seconds) and similar to PlaceNet. Therefore, despite the higher FLOPs, the computational complexity of our method is manageable and affordable, with efficient real-world inference times.

8. Loss function analysis

In Figure 13, we compare the impact of various loss functions. The regression loss, with sparse annotation, poses challenges in training the model effectively. Gaussian assigned loss overlooks the impact of scaling and fails to accommodate multi-peak distributions for possible placements. Sparse contrastive loss supports the fluctuation of neighboring placements but lacks accurate constraints for complex scenes with location-varying placements. Our proposed loss function is derived from bounding box loss using Generalized IOU loss, offering more precise constraints on box scaling.

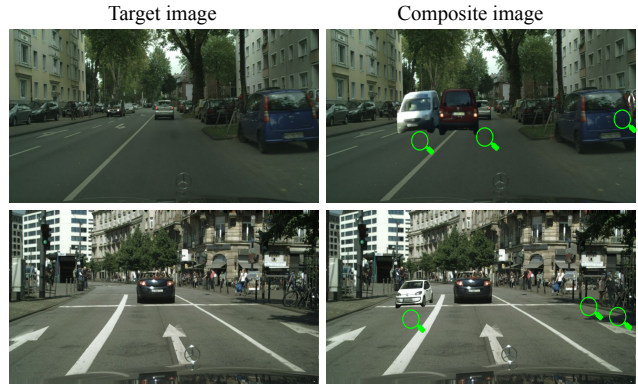


Figure 12. **Multi-object placement.** Two cars and one person (top), one car and two people (below) are composed into the scene.

9. Multi-object placement

Compared to single-object placement, multi-object placement is significantly more challenging as it necessitates an understanding of the prior state of composed objects, scene objects and background image. Though our network makes parallel bounding box predictions, it has learned a robust correspondence between objects and their associated regions. In Figure 12, we illustrate the potential for composing three objects into street scenes, showing the capability of our network to learn object orientation and the distribution of various object categories.

10. Dataset construction

In Figure 14, we illustrate the data construction process for the Cityscapes [11] dataset, which is applicable to other datasets. We start with the source image ① and employ a pretrained MaskFormer [9] model for panoptic semantic segmentation ②, jointly performing semantic and instance segmentation. Scene primitives are manually categorized into object classes, including car, person, rider, train, bus, bicycle, truck, motorcycle, resulting in binary object masks ③. To obtain object-free backgrounds, we dilate the binary object masks to address boundary inaccuracies and obtain dilated object masks ④. The next step involves using pretrained LaMa [41] inpainting model to remove objects, yielding inpainted images ⑦. As many segmentation models tend to classify shadows as background, we manually remove these shadows using an online PhotoKit tool, refining the background image to obtain corrected inpainted images ⑧. Simultaneously, we create an object pool ⑤ consisting of both intact objects

	PlaceNet (ECCV'20) [51]	SAC-GAN (IEEE TVCG'22) [53]	TopNet (CVPR'23) [55]	BOOTPLACE (ours)
# Params (M)	35.9	35.9	25.0	41.4
# FLOPs (G)	4.40	6.96	6.79	44.4
Inference time (sec)	0.68	0.1	2.7	0.27

Table 4. Comparison of computational cost and model parameters tested on Cityscapes dataset.

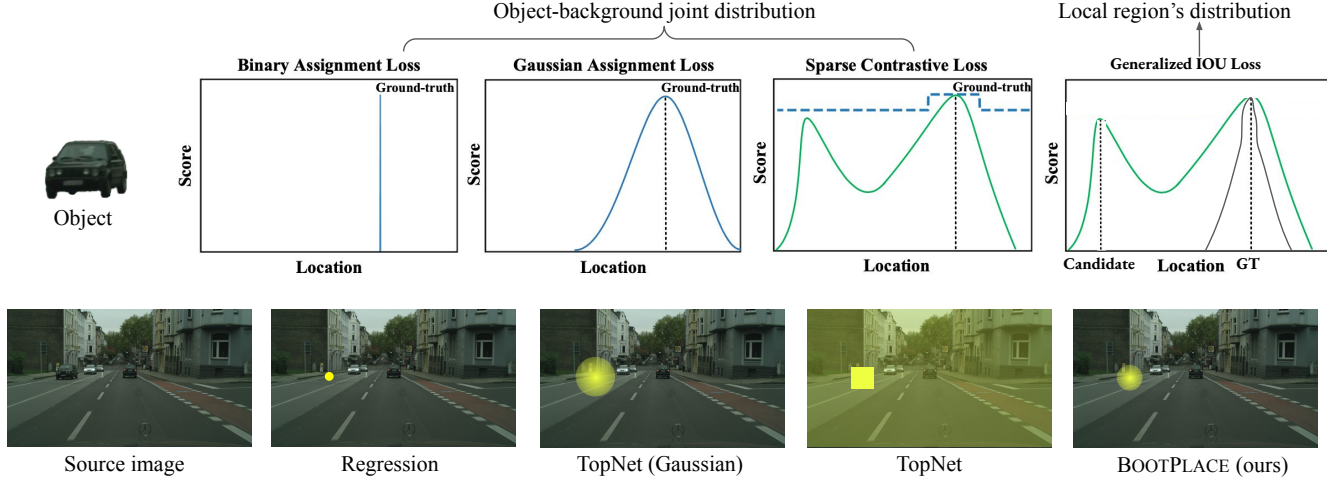


Figure 13. **Different losses** exemplified in 1D space. The yellow marks, depicted with varying intensities, represent the constraint intensity.

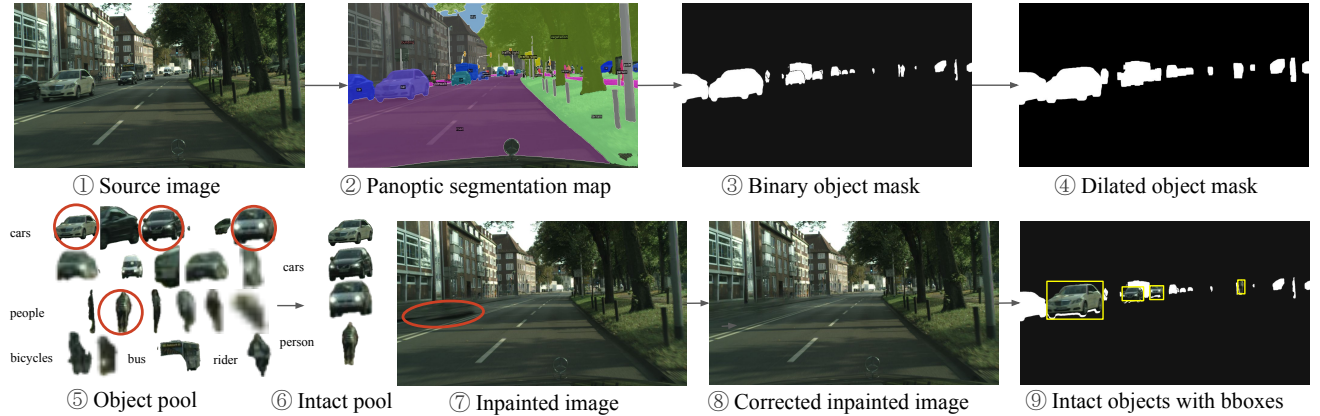


Figure 14. **Data preparation** of background inpainted images and corresponding scene objects processed from source images.



Figure 15. **Data preparation** for boundary harmonization. The boundary dilated regions are automatically segmented by dilation of object silhouette.

and those that are partially occluded, each with varying resolutions. After manual curation, we retain only the intact objects, resulting in an intact object pool ⑥ with their bounding box coordinates. After data cleaning, we construct a multi-object dataset including 2,953 training images with 22,270 objects and their corresponding ground-truth labels, as well as 372 testing images with 2,713 objects.



Figure 16. **Harmonization results** of composite Cityscapes samples. Zoom in to see visual details.

	TopNet	BOOTPLACE (Ours)
Encoder	ViT-small	CNN + MLP + Transformer encoders
Decoder	2D upsampling	Transformer decoder + MLPs
Output	3D heatmap	Bbox + class predictions
Losses	Sparse contrastive + range	Bbox regression + class prediction + association
Training	AdamW optimizer + lr=1e-5	AdamW optimizer + lr= 4e-4

Table 5. TopNet vs BOOTPLACE (ours).



Figure 17. Comparison of w/o (row 1 and 3) vs w/ (row 2 and 4) object compositing for two examples on object replacement task.

11. Method comparison with TopNet

We provide comparisons between TopNet and BOOTPLACE in architecture and training strategy in Table 5.

12. Image blending

To address boundary artifacts arising from copy-paste object composition, we employ two distinct methods: (1) use a diffusion model initially designed for image inpainting to harmonize boundaries. We finetune the Stable Diffusion Inpainting model without prompt conditioning² on Cityscapes objects. This involves extracting object-centric patches and dilating their masks to create boundary masks, as depicted in Figure 15. Once a sufficient number of such

²<https://github.com/lorenzo-stacchio/Stable-Diffusion-Inpaint/tree/1b44f2f9e4f233f68d48c56b68b9c111c1538d4d>

	Copy-paste		ObjectStitch		Scale
	FID (↓)	LPIPS (↓)	FID (↓)	LPIPS (↓)	
PlaceNet [51]	52.02	0.088	77.67	0.217	0.204
SAC-GAN [53]	42.89	0.066	63.44	0.194	0.156
TopNet [55]	38.21	0.043	49.74	0.189	0.079
BOOTPLACE (ours)	58.74	0.105	79.50	0.246	0.310

Table 6. Quantitative comparison using FID and LPIPS.

patch-mask pairs are collected, we finetune the model to harmonize boundary region. Figure 16 shows the visual performance of image harmonization on Cityscapes samples. (2) combine placement learning with identity-preserving compositing methods such as ObjectStitch [40] for visual refinement, as shown in Figure 17. This process significantly reduces boundary artifacts while naturally generating shadows, resulting in an enhanced level of realism compared to compositions without harmonization.

13. Evaluation on FID and LPIPS

In Table 6, we evaluate plausibility of composite images using FID and LPIPS on the Cityscapes dataset. We observe that both metrics are strongly correlated with bbox scale, where smaller bounding boxes result in fewer modifications to the image and correspondingly lower FID and FPIPS values. Therefore, they are not suitable metrics for evaluating placement quality, which are excluded from evaluation.

14. More qualitative results

We show qualitative results of object placement on Cityscapes dataset in Figures 18 and 19, object reposition on Cityscapes dataset in Figures 20 and 21, and object reposition on OPA dataset in Figure 22.

15. More decoder attention visualization

We provide additional visualization results showing the distribution of the detection decoder in Figure 23.



Figure 18. **Qualitative results of single object placement** on Cityscapes dataset. Objects are randomly chosen from its testing set.



Figure 19. **Qualitative results of object placement** on Cityscapes dataset. Objects are randomly chosen from its testing set.



Figure 20. **Qualitative results of object reposition** on Cityscapes dataset.



Figure 21. **Qualitative results of object reposition** on Cityscapes dataset.

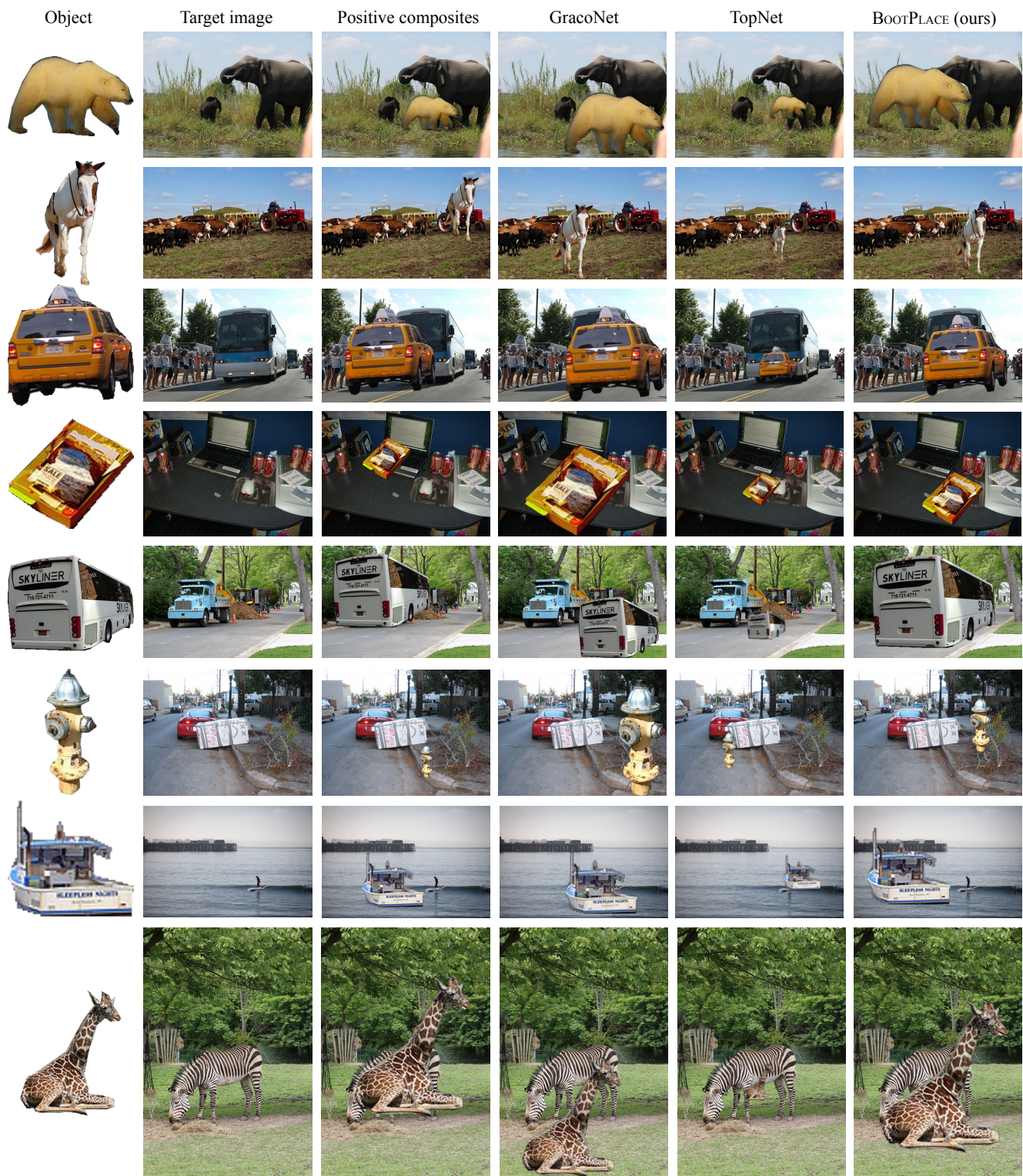


Figure 22. Qualitative results of object reposition on OPA dataset.



Figure 23. **Decoder attention visualization** of Cityscapes samples.